Original Article
The molecular mechanism underlying angiogenesis in a mouse model of chronic kidney disease after ischemic stroke

Fang Wang[2*], Liangxiang Lu[1*], Jialun Feng[1], Jinhua Zheng[1], Zefeng Wei[1], Ziqiang Wang[1]

[1]Department of Nephrology, The First Affiliated Hospital of Hainan Medical University, Haikou 570102, Hainan, China; [2]Ganzhou People's Hospital (Nanfang Hospital, Ganzhou), Ganzhou 341000, Jiangxi, China. *Equal contributors and co-first authors.

Abstract: Objectives: The study aims to establish a reliable chronic kidney disease (CKD) mouse model by examining the effects of an adenine-containing diet on renal function and pathology. It also explores the impact of CKD on motor function and infarct volume following cerebral infarction and investigates the role of calcium in modulating the AMPK/SIRT1/HIF1-α signaling pathways. Method: The CKD mouse model was induced through an adenine-enriched diet. Renal function impairment was assessed by analyzing blood samples for creatinine and blood urea nitrogen levels at 0 and 6 weeks. Pathologic changes in renal tissue were examined. The study also evaluated motor function, infarct volume, survival rates, body weight changes, and functional assessments. Additionally, cerebral cortex angiogenesis was assessed in the context of ischemic stroke. Result: The CKD mouse model showed significant renal tissue alterations, including luminal dilation, glomerular hypertrophy, fibrosis, and inflammatory infiltration. There was a notable reduction in angiogenic markers in the CKD group compared to controls. The study also found increased cerebral calcium levels and altered expression of AMPK, SIRT1, HIF1-α, and VEGF in the CKD group. Conclusions: The research successfully created the CKD mouse model and emphasized the disease's many effects, including its influence on neurological disorders. The results provide an understanding of the molecular processes behind changes brought on by CKD and may have consequences for angiogenesis and signaling pathway-focused therapeutic approaches.

Keywords: AMPK, ischemic stroke, angiogenesis, CKD

Introduction

CKD is a prevalent condition characterized by the progressive deterioration of renal function [1], often leading to systemic complications [2]. In recent years, a growing body of data has indicated a correlation between CKD and stroke as well as cerebrovascular disease [3]. Specifically, CKD has been found to elevate the risk and severity of ischemic stroke [4].

Ischemic stroke is the primary factor contributing to adult disability on a global scale [5]. Angiogenesis that occurs without external intervention following the acute phase of stroke may enhance neurological function improvement [6-8]. Angiogenesis, also known as neovascularization, is particularly noticeable in the area around the ischemic region and is associated with decreased brain injury [8]. Vascular endothelial growth factor (VEGF) is an angiogenic factor [9] that promotes the formation of new cerebral blood vessels [10]. Therefore, VEGF also plays a crucial role in determining the size of ischemic cerebral infarction and the extent of neurological damage. Some researchers have shown that individuals with CKD often have abnormal VEGF expression, which may impact the effectiveness of blood vessel formation after a stroke [11]. This imbalance may result in a compromised capacity to generate new blood vessels in response to ischemic events.

In this study, we created a transient middle cerebral artery occlusion (tMCAO) in a CKD
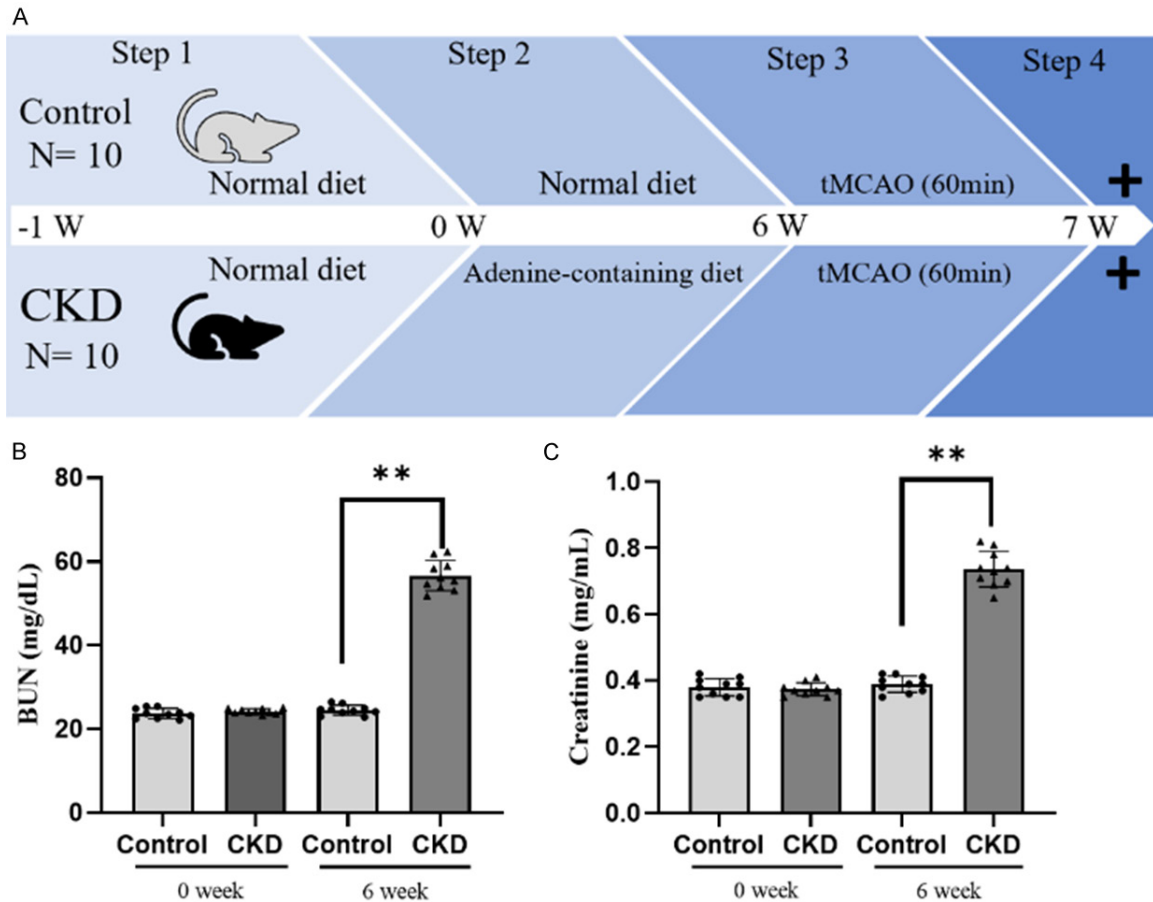
Figure 1. (A) The control and CKD groups were included in the experimental groupings. During weeks 1 through 6, meals containing the known hazard adenine were provided to the mice in the CKD group. During week 7, the mice were transitioned to a diet devoid of adenine. Then, behavioral evaluations were carried out. To compare BUN and creatinine levels prior to and after the adenine-containing diet was administered, serum samples were obtained at weeks 0 and 6. (B) Measurements of serum BUN and (C) creatinine levels were obtained at weeks 0 and 6. **P < 0.01, vs the CKD group. The experiment was independently repeated three times. CKD, chronic kidney disease; BUN, blood urea nitrogen; tMCAO, transient middle cerebral artery occlusion.

mouse model. The study emphasizes the intricate relationship between CKD and angiogenesis. This impairment in blood vessel function would not only contribute to the advancement of chronic renal disease but also greatly enhance the vulnerability to cerebrovascular incidents, such as ischemic stroke [12]. Exploration of the complicated relationship among CKD, ischemic stroke, and angiogenesis, especially VEGF-mediated mechanisms, will allow for tailored treatments. VEGF modulation or angiogenic responses may reduce stroke consequences in CKD patients, providing new paths for neurologic outcomes in this high-risk group. Understanding these interrelationships will help create improved preventative and treatment methods for CKD and ischemic stroke patients as research in this field advances.

Materials and methods

Establishment of the CKD mouse model

Adult male C57BL/6J mice, 8 weeks old and weighing 22-30 g, were kept in separate cages in a facility with regulated temperature (22-25°C), humidity (45-50%), and lighting conditions (12 hours of light followed by 12 hours of darkness). Before developing CKD (**Figure 1A**), all mice were given a conventional diet and had free access to food and water for 1 week. CKD was induced by administering a meal enriched in adenine, whereas the control animals received a standard diet. Before providing the

adenine-containing food, a small amount of blood was collected from the cheek by micro-tube puncture. The serum was then separated by centrifugation at a force of 1,500×g for 10 minutes at 4°C. Afterward, the mice were randomly allocated into two groups. The control group (n = 10) received a standard diet. In the CKD group (n = 10), mice were administered an adenine diet containing 0.2% w/w adenine (A2786, Sigma-Aldrich, St. Louis, MO, USA). After 6 weeks (**Figure 1A**), blood samples were collected and then centrifuged to obtain serum. The serum samples were examined to evaluate the concentrations of blood urea nitrogen (BUN) and creatinine before and after the ingestion of a meal containing adenine.

Detection of serum biochemical indexes

At 0 and 6 weeks, blood samples were collected from the mice after an 8-12-hour period of fasting and then analyzed by biochemical testing. The blood samples underwent centrifugation at 1,500×g to separate the serum. The purified serum was then kept at a temperature of -80°C for preservation. The levels of BUN (EIABUN, Invitrogen) and creatinine (ab65340, Abcam, Cambridge, UK) were measured using the appropriate methods. Renal function test results were used to assess the efficacy of CKD model construction.

Establishment of tMCAO

All mice chosen for the control and CKD groups received tMCAO surgery (**Figure 1A**). A mixture of nitrous oxide, oxygen, and isoflurane (69%:30%:1%) was delivered via an inhalation mask to anesthetize the mice. When the mice were anesthetized, the oxygen supply was discontinued, and only isoflurane was administered to suppress mouse respiration until death. The mice were given an anesthetic to relieve pain. The right carotid bifurcation was revealed, and the external carotid artery was ligated proximal to the bifurcation. Next, a 7-0 nylon filament thread, coated with silicon, was inserted into the right common carotid artery to block the right middle cerebral artery (MCA). Following 60 minutes of tMCAO, the nylon thread was gradually removed to restore blood flow in the MCA. All animals were euthanized 7 days after the procedure. The sample size was

determined using preliminary study findings. To achieve a statistical power of 80% and a significance level of 5%, a sample size of eight mice in each group was required to detect a reduction in stroke volume between the control and CKD groups. This calculation considered an anticipated dropout rate of 10%. A total of 20 mice were utilized for this study. However, six mice from all groups were excluded due to specific exclusion criteria. These mice died after surgery and before the sacrifice time (n = 2). Immunostaining was performed on a control group consisting of five mice and a CKD group consisting of four mice. Western blotting was conducted on a control group of four mice and a CKD group of four mice.

Neurobehavioral analysis

The body weight of mice in each group was measured 7 days after tMCAO and before they were sacrificed. The neurological tests included Bederson's score, as well as corner and rotarod tests, which were performed in a double-blinded manner. The mice were assessed both before and 7 days after tMCAO. Bederson's score [13], with minor modifications [14], was evaluated in the following manner: 0 indicated the absence of any noticeable neurological impairments; 1 signified the inability to extend the left forepaw fully; 2 referred to the tendency to move in a circular motion toward the opposite side; 3 denoted a tendency to tumble toward the left side; 4 indicated an inability to walk without external assistance. The rotarod test (MK610A; Muromachi Kikai Co., Tokyo, Japan), conducted according to our previous publications, assessed motor coordination integrity [15].

Tissue preparation

A mixture of nitrous oxide, oxygen, and isoflurane (69%:30%:1%) was delivered via an inhalation mask to anesthetize the mice. When the mice were anesthetized, we injected pentobarbital (40 mg/kg) intraperitoneally to the mice. Then, the 20 ml of ice-cold phosphate-buffered saline (PBS) was perfused by heart. Next, mice that were used for immunostaining were perfused with 20 ml of ice-cold 4% paraformaldehyde (PFA) in 0.1 mol/L phosphate buffer. The brains and kidneys were removed and post-

fixed in 4% PFA overnight. After washing with PBS, the tissues were immersed in sucrose solutions with concentrations of 10%, 20%, and 30% (w/v). Subsequently, the tissues were encased in dry ice and frozen at -80°C. The tissues were sectioned using a cryostat at -24°C, placed onto glass slides coated with silicon, and stored at -80°C.

Protein samples were obtained from remaining mouse cerebral tissues using radioimmunoprecipitation assay (RIPA) lysis buffer, which contained protease inhibitors. The RIPA lysis solution was obtained from Beyotime. The protein concentration was determined using a bicinchoninic acid kit (20201ES76, Yeasen Company, Shanghai, China), and the samples were stored at -80°C.

Histopathological staining

To measure the volume of the infarct, coronal brain slices were treated with cresyl violet for Nissl staining and visualized using a light microscope (SZX-12; Olympus Optical Co., Tokyo, Japan). The sections were dissected at distances of 1.0, 0.5, 0, -0.5, and -1.0 mm from the bregma. The infarct area was quantified in five distinct sections by pixel counting using image processing software (ImageJ; National Institutes of Health, Bethesda, MD, USA). The infarct volume was then determined by summing the infarct volumes into five consecutive brain sections spaced 0.5 mm apart.

The kidney sections were stained using hematoxylin and eosin (H&E), a Masson trichrome stain kit (1004850001, Sigma), and a periodic acid-Schiff (PAS) reagent (ab150680, Abcam) according to the manufacturer's instructions. After applying neutral gum as a sealer, the sections were inspected and recorded using an inverted microscope (SZX-12; Olympus Optical, Tokyo, Japan). The morphological assessments were carried out autonomously by two proficient pathologists using a double-blind methodology.

Immunofluorescence

To evaluate angiogenesis in the mouse brain after cerebral infarction, we employed an immunofluorescence double-labeling technique to detect the expression of CD31 and Ki67.

The double-immunofluorescence analysis utilized a goat anti-CD31 antibody (1:500; R&D Systems, AF3628) and a rabbit anti-Ki67 antibody (1:500; Abcam, ab15880) as the primary antibodies.

To observe the immune response, the appropriate fluorescent secondary antibodies, an Alexa 488-coupled rabbit anti-goat IgG antibody (Thermo Fisher Scientific) and an Alexa 555-coupled goat anti-rabbit antibody were employed. The sections were examined at 200× magnification using a confocal microscope (LSM-510; Zeiss, Jena, Germany).

Western blot analysis

Various protein concentrations were assessed. The proteins underwent separation using sodium dodecyl sulfate-polyacrylamide gel electrophoresis and were subsequently transferred by electrophoresis onto a polyvinylidene fluoride membrane (IPVH85R, Millipore, Germany). The membrane was blocked for 1 hour using a 5% solution of bovine serum albumin. Subsequently, it was subjected to incubation with the following primary antibodies: rabbit anti-phospho-AMPKα (2535, 1:1000, Cell Signaling Technology), rabbit anti-SIRT1 (sc15404, 1:1000, Santa Cruz Biotechnology), rabbit anti-HIF1-α (20960-1-AP, 1:1000, Proteintech), rabbit anti-VEGF (ab46154, 1:2000, Abcam), and anti-β tubulin (ab6046, 1:1000, Abcam) at 4°C overnight. Afterward, the membrane underwent three washes with Tris-buffered saline with Tween-20 (TBST), each lasting 5 minutes. This was followed by a 1-hour incubation with horseradish peroxidase (HRP)-conjugated secondary antibody, specifically rabbit anti-mouse IgG (AS029, ABclonal), which was diluted at a ratio of 1:2000. Following the TBST rinses, the membrane was treated with luminous liquid for development. The data were examined using ImageJ software. Protein expression was quantified by calculating the ratio of the gray value of the protein being tested to that of the internal reference (β-tubulin).

Enzyme-linked immunosorbent assay (ELISA)

Mouse brain protein samples were obtained by centrifugation at 1,000×g for 10 minutes at 4°C and directly collected. Calcium (Ca^{2+}) levels were determined using an ELISA kit
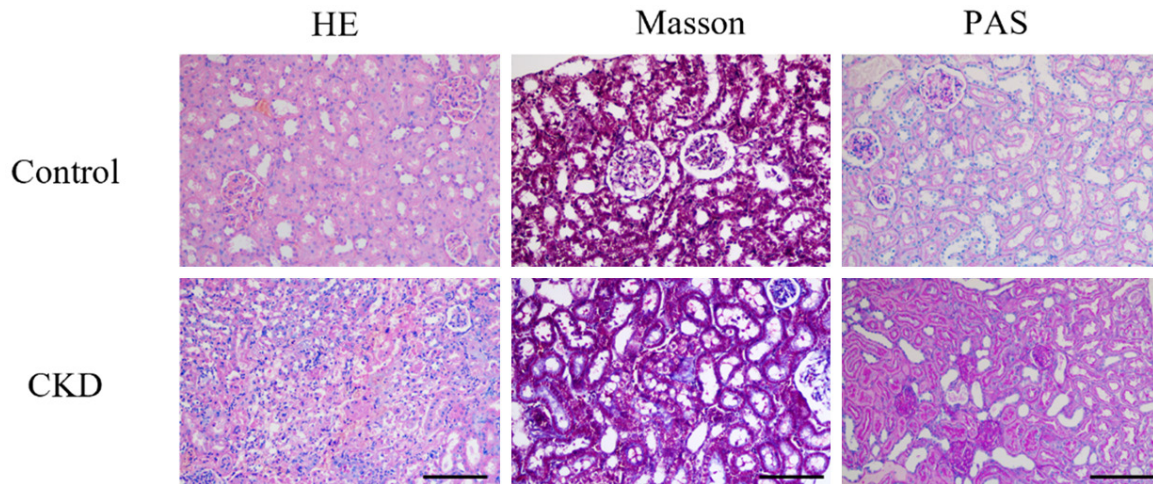
Figure 2. Representative Masson, PAS, and H&E images of kidney sections from mice (scale bar = 50 μm). Significant enlargement of the tubular lumen and glomeruli was observed in the mice assigned to the CKD group compared with that in animals of the control group. HE, hematoxylin and eosin; PAS, periodic acid-Schiff.

(Calcium Assay Kit; Catalog No. ab102505; Abcam). Then, 50 μl of the standard sample, at the specified concentration, was dispensed into the designated wells as per the manufacturer's guidelines. Additionally, 10 μl of the brain protein sample was added to the sample wells, followed by 40 μl of the dilution solution. The detection antibody tagged with HRP (100 μl) was added to the standard and sample wells. The plate was securely covered and incubated for 1 hour. Following five washes, Substrate A and B (50 μl each) were added to the wells, and the plate was incubated at 37°C for 15 minutes. Then, 50 μl of termination solution was dispensed into each well, and the optical density was measured at 450 nm after 15 minutes.

Statistical analysis

All data were analyzed using GraphPad Prism. Measurement data are expressed as the mean ± standard deviation. An unpaired t-test was used to compare data between the two groups. A value of *P* < 0.05 was considered statistically significant.

Results

Renal function impairment caused by an adenine diet

Because creatinine and serum BUN are indicators of renal dysfunction [4], we assessed

whether renal function was compromised after administering an adenine diet. In this experiment, we obtained blood samples at two distinct time periods, namely 0 and 6 weeks, to conduct a comparison. Within the CKD group, the levels of BUN exhibited a notable escalation from the 0-week to the 6-week time points (**Figure 1B**), and there was a considerable elevation in the creatinine level between the 0-week and 6-week time points (**Figure 1C**). The control group showed no change in the levels of BUN and creatinine from 0 to 6 weeks.

Pathologic changes in renal tissue of CKD mice

Mice in the normal diet group had normal renal histology with intact tubular epithelial cells and no obvious pathological changes in the glomeruli and renal interstitium. However, mice fed an adenine-containing diet demonstrated dilated renal lumens and glomerular hypertrophy, as well as marked fibrosis, tubular epithelial cell edema, and interstitial inflammatory infiltration (**Figure 2**). These results suggest that the CKD mouse model was successfully constructed.

Motor function and infarct volume

The survival rates at 7 days following reperfusion were 90% (n = 9) and 80% (n = 8) for animals in the control and CKD groups, respectively (**Figure 3A**). There was no notable dispar-
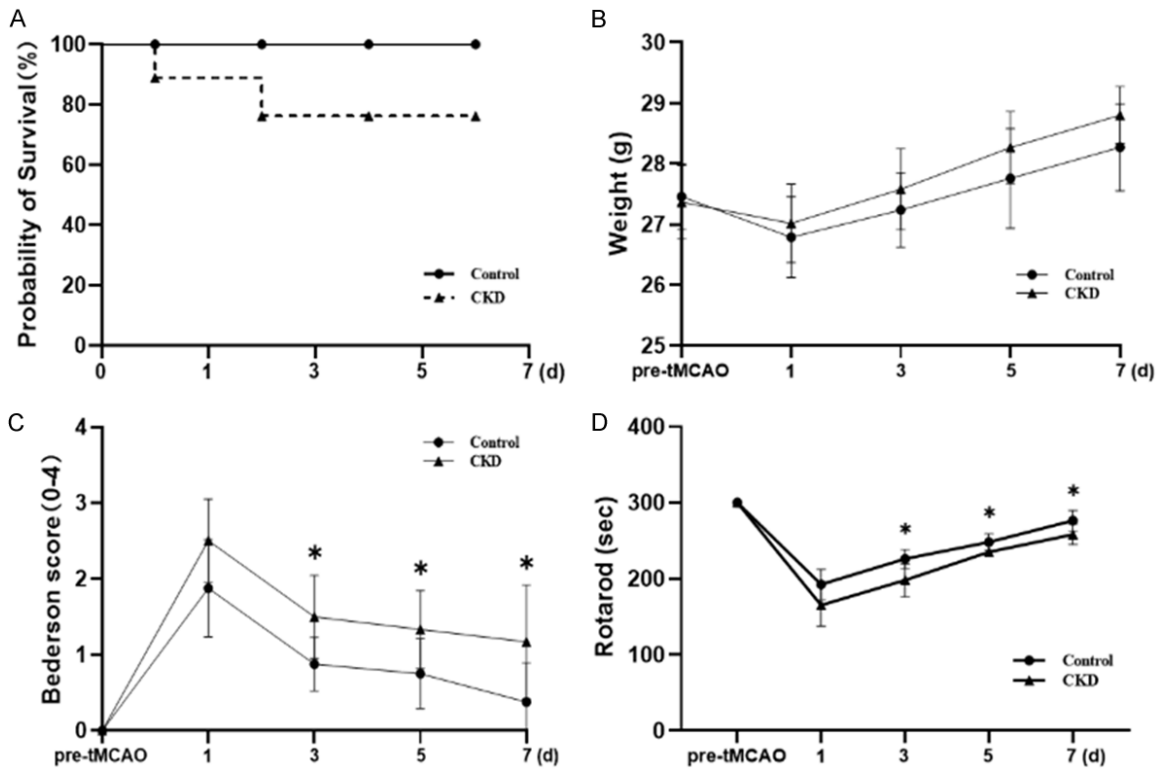
Figure 3. Neurobehavioral analysis of mice after tMCAO. A. The survival rates for 7 days after tMCAO (until sacrifice) in the control and CKD groups were 90% and 80%, respectively (not significantly different). B. There was no significant difference in body weight between the control and CKD groups. C. The Bederson score of the CKD group was significantly lower than that of the control group at the 3-day, 5-day, and 7-day time points. D. The CKD group exhibited notably lower rotarod test scores than those of the control group at the 3-day, 5-day, and 7-day time points. *$P < 0.05$, vs the CKD group.
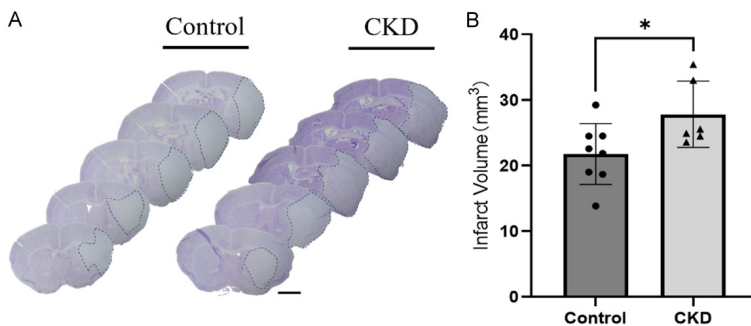
Figure 4. Infarct volume of mice after tMCAO. A. Nissl staining of mouse brain sections from the control and CKD groups after tMCAO. Scale bar = 2 mm. B. Quantitative analysis of infarct volume in the two groups. Note the significant increase in infarct volume in the CKD group compared with that in the control group (*$P = 0.0384$, vs the CKD group).

An assessment of infarct volume was performed using Nissl staining (**Figure 4A**). There was a significant difference in the infarct volume between the control and CKD groups (*$P = 0.0384$ vs the CKD group, Friedman test, **Figure 4B**).

Ca^{2+} controls the production of VEGF by facilitating communication among the AMPK/SIRT1/HIF1-α signaling pathways

By analyzing the Ca^{2+} levels in the brains of mice after cerebral infarction, we observed a significant increase in the brains of mice in the CKD group (**Figure 5A**, **$P = 0.0025$, vs the CKD group). This outcome is identical to the finding of a previous study [16]. In the **Figure 5B**, the CKD

ity in body weight between the two groups over 7 days (**Figure 3B**). However, there was a noteworthy difference in Bederson's score and the rotarod test results between the two groups starting from day 7 (**Figure 3C**, **3D**).
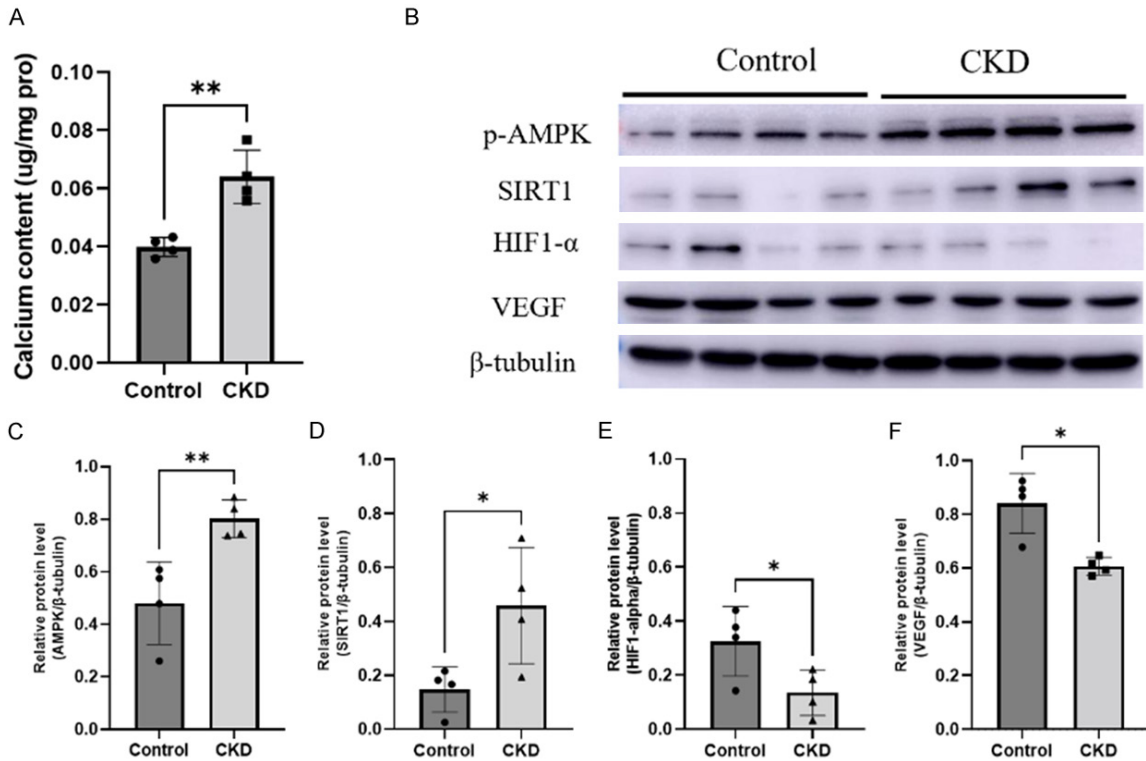
Figure 5. A. The concentration of Ca^{2+} in mouse brain tissue was quantified using the ELISA technique. B. Expression of AMPK, SIRT1, HIF1-α, and VEGF in the brain tissue of both the control and CKD groups was detected using western blotting, and β-tubulin was used as a control. C-F. Quantitative analysis of the expression of AMPK, SIRT1, HIF1-α, and VEGF in the two groups *P < 0.05, vs the CKD group. The experiment was independently repeated three times. p-AMPK, phosphorylated AMP-activated protein kinase; SIRT1, Silent Information Regulator 2 Related Enzyme 1; HIF1-α, Hypoxia-Inducible Factor 1-Alpha; VEGF, vascular endothelial growth factor.

group showed significant increases in the expression of AMPK (**Figure 5C**, *P = 0.0097, vs the CKD group) and SIRT1 (**Figure 5D**, *P = 0.0361, vs the CKD group), whereas the expression of HIF1-α (**Figure 5E**, *P = 0.0487, vs the CKD group) and VEGF (**Figure 5F**, *P = 0.0286, vs the CKD group) was significantly reduced compared with that in the control group.

Detection of mouse cerebral cortex angiogenesis using CD31/Ki67

After an ischemic stroke, the growth of new blood vessels (angiogenesis) takes place in the areas around the damaged tissue (peri-infarct regions). This process has been shown to have a beneficial relationship with the survival and recovery of experimental animals [17]. Therefore, in this investigation, we used CD31 and Ki67 immunofluorescence to examine angiogenesis in the vicinity of the central region of cerebral infarction in mice (**Figure 6A**). The CKD group had significantly reduced expression of

CD31 and Ki67 compared with that in the control group (**Figure 6B**, *P = 0.0202, vs the CKD group).

Discussion

Disruption of Ca^{2+} ions is a characteristic feature of CKD and a significant risk factor for the occurrence of severe cardiovascular consequences [18]. The present study elucidates the impact of CKD on the control of Ca^{2+}. Our findings indicate that an experimental model of renal failure produced comparable classical characteristics of CKD. The CKD model led to elevated Ca^{2+} expression in the brains of mice, thereby causing enlargement of cerebral infarcts and a decline in the motor performance of mice. These results have significance for better understanding the relationship between kidney disease and cerebrovascular accidents.

The CKD group had elevated levels of BUN and creatinine after 6 weeks of an adenine diet,

Figure 6. A. The images show expression of CD31 and Ki67 in the ischemic hemisphere, captured from both the control and CKD groups on the 7th day after ischemia and reperfusion. Scale bar = 100 µm. B. Measurement of CD31/Ki67 levels. The results are presented as the mean ± standard deviation and were evaluated using a t-test. *P < 0.05, vs the CKD group. CD31, Cluster of Differentiation 31.

suggesting a decline in renal function. The findings align with prior research and validate the dependability of the CKD mouse model [19]. The increase in cerebral Ca^{2+} levels after cerebral infarction in the CKD group indicates the possible involvement of Ca^{2+} in regulating signaling pathways. Ca^{2+} that is released from spaces outside of cells or compartments inside cells and enters the cytosol triggers calmodulin activation. Calmodulin then attaches to calmodulin-dependent protein kinase kinase (CaMKK) and calmodulin-dependent protein kinase (CaMK), stimulating their production [20]. Activation of CaMKK enhances the activity of AMPK via modulation of the CaMK protein located downstream [21]. AMPK activation enhances the NAD^+:NADH ratio, thereby increasing SIRT1 activity [22], resulting in reduced HIF1-α expression [23]. Nevertheless, the heightened expression of HIF1 stimulates upregulation of VEGF [24], a crucial protein implicated in the angiogenesis process [25]. The decreased CD31/Ki67 positivity in the CKD group, compared with that in the control group, indicates a compromised ability to form new blood vessels in response to cerebral infarction. The weakening of the angiogenic process in the CKD group may lead to hindered recovery after a stroke. Diminished formation of new blood vessels in the area around the damaged tissue after a stroke may play a crucial role in the survival and recuperation of animals with impaired kidney function.

Collectively, our findings underscore the intricate connection among renal impairment caused by an adenine diet, cerebrovascular events, and the associated molecular pathways. Additional research is required to comprehensively determine the underlying pathophysiological mechanisms connecting renal damage and neurological outcomes. This research will also provide novel insights into the management of renal dysfunction that occurs as a complication of ischemic stroke.

Disclosure of conflict of interest

None.

Abbreviations

CKD, chronic kidney disease; VEGF, Vascular endothelial growth factor; tMCAO, transient middle cerebral artery occlusion; BUN, blood urea nitrogen; MCA, middle cerebral artery; PFA, paraformaldehyde; RIPA, radioimmunoprecipitation assay; H&E, hematoxylin and eosin; PAS, periodic acid-Schiff; TBST, Tris-buffered saline with Tween; HRP, horseradish peroxidase; ELISA, Enzyme-linked immunosorbent assay; Ca^{2+}, Calcium; CaMKK, calmodulin-dependent protein kinase kinase; CaMK, calmodulin-dependent protein kinase.

Address correspondence to: Zefeng Wei and Ziqiang Wang, Department of Nephrology, The First Affiliated Hospital of Hainan Medical University,

Haikou 570102, Hainan, China. E-mail: wzf5866-08@163.com (ZFW); ziqiangwang1986@163.com (ZQW)

References

[1] Kovesdy CP. Epidemiology of chronic kidney disease: an update 2022. Kidney Int Suppl (2011) 2022; 12: 7-11.

[2] Thomas R, Kanso A and Sedor JR. Chronic kidney disease and its complications. Prim Care 2008; 35: 329-344, vii.

[3] Toyoda K and Ninomiya T. Stroke and cerebrovascular diseases in patients with chronic kidney disease. Lancet Neurol 2014; 13: 823-833.

[4] Kelly D and Rothwell PM. Disentangling the multiple links between renal dysfunction and cerebrovascular disease. J Neurol Neurosurg Psychiatry 2020; 91: 88-97.

[5] GBD 2016 Lifetime Risk of Stroke Collaborators, Feigin VL, Nguyen G, Cercy K, Johnson CO, Alam T, Parmar PG, Abajobir AA, Abate KH, Abd-Allah F, Abejie AN, Abyu GY, Ademi Z, Agarwal G, Ahmed MB, Akinyemi RO, Al-Raddadi R, Aminde LN, Amlie-Lefond C, Ansari H, Asayesh H, Asgedom SW, Atey TM, Ayele HT, Banach M, Banerjee A, Barac A, Barker-Collo SL, Bärnighausen T, Barregard L, Basu S, Bedi N, Behzadifar M, Béjot Y, Bennett DA, Bensenor IM, Berhe DF, Boneya DJ, Brainin M, Campos-Nonato IR, Caso V, Castañeda-Orjuela CA, Rivas JC, Catalá-López F, Christensen H, Criqui MH, Damasceno A, Dandona L, Dandona R, Davletov K, de Courten B, deVeber G, Dokova K, Edessa D, Endres M, Faraon EJA, Farvid MS, Fischer F, Foreman K, Forouzanfar MH, Gall SL, Gebrehiwot TT, Geleijnse JM, Gillum RF, Giroud M, Goulart AC, Gupta R, Gupta R, Hachinski V, Hamadeh RR, Hankey GJ, Hareri HA, Havmoeller R, Hay SI, Hegazy MI, Hibstu DT, James SL, Jeemon P, John D, Jonas JB, Jóźwiak J, Kalani R, Kandel A, Kasaeian A, Kengne AP, Khader YS, Khan AR, Khang YH, Khubchandani J, Kim D, Kim YJ, Kivimaki M, Kokubo Y, Kolte D, Kopec JA, Kosen S, Kravchenko M, Krishnamurthi R, Kumar GA, Lafranconi A, Lavados PM, Legesse Y, Li Y, Liang X, Lo WD, Lorkowski S, Lotufo PA, Loy CT, Mackay MT, Abd El Razek HM, Mahdavi M, Majeed A, Malekzadeh R, Malta DC, Mamun AA, Mantovani LG, Martins SCO, Mate KK, Mazidi M, Mehata S, Meier T, Melaku YA, Mendoza W, Mensah GA, Meretoja A, Mezgebe HB, Miazgowski T, Miller TR, Ibrahim NM, Mohammed S, Mokdad AH, Moosazadeh M, Moran AE, Musa KI, Negoi RI, Nguyen M, Nguyen QL, Nguyen TH, Tran TT, Nguyen TT, Anggraini Ningrum DN, Norrving B, Noubiap JJ, O'Donnell MJ, Olagunju AT, Onuma OK, Owolabi MO, Parsaeian M, Patton GC, Piradov M, Pletcher MA, Pourmalek F, Prakash V, Qorbani M, Rahman M, Rahman MA, Rai RK, Ranta A, Rawaf D, Rawaf S, Renzaho AM, Robinson SR, Sahathevan R, Sahebkar A, Salomon JA, Santalucia P, Santos IS, Sartorius B, Schutte AE, Sepanlou SG, Shafieesabet A, Shaikh MA, Shamsizadeh M, Sheth KN, Sisay M, Shin MJ, Shiue I, Silva DAS, Sobngwi E, Soljak M, Sorensen RJD, Sposato LA, Stranges S, Suliankatchi RA, Tabarés-Seisdedos R, Tanne D, Nguyen CT, Thakur JS, Thrift AG, Tirschwell DL, Topor-Madry R, Tran BX, Nguyen LT, Truelsen T, Tsilimparis N, Tyrovolas S, Ukwaja KN, Uthman OA, Varakin Y, Vasankari T, Venketasubramanian N, Vlassov VV, Wang W, Werdecker A, Wolfe CDA, Xu G, Yano Y, Yonemoto N, Yu C, Zaidi Z, El Sayed Zaki M, Zhou M, Ziaeian B, Zipkin B, Vos T, Naghavi M, Murray CJL and Roth GA. Global, regional, and country-specific lifetime risks of stroke, 1990 and 2016. N Engl J Med 2018; 379: 2429-2437.

[6] Liu J, Wang Y, Akamatsu Y, Lee CC, Stetler RA, Lawton MT and Yang GY. Vascular remodeling after ischemic stroke: mechanisms and therapeutic potentials. Prog Neurobiol 2014; 115: 138-156.

[7] Kanazawa M, Takahashi T, Ishikawa M, Onodera O, Shimohata T and Del Zoppo GJ. Angiogenesis in the ischemic core: a potential treatment target? J Cereb Blood Flow Metab 2019; 39: 753-769.

[8] Krupinski J, Kaluza J, Kumar P, Kumar S and Wang JM. Role of angiogenesis in patients with cerebral ischemic stroke. Stroke 1994; 25: 1794-1798.

[9] Leung DW, Cachianes G, Kuang WJ, Goeddel DV and Ferrara N. Vascular endothelial growth factor is a secreted angiogenic mitogen. Science 1989; 246: 1306-1309.

[10] Rosenstein JM, Mani N, Silverman WF and Krum JM. Patterns of brain angiogenesis after vascular endothelial growth factor administration in vitro and in vivo. Proc Natl Acad Sci U S A 1998; 95: 7086-7091.

[11] Tanaka S, Tanaka T and Nangaku M. Hypoxia and dysregulated angiogenesis in kidney disease. Kidney Dis (Basel) 2015; 1: 80-89.

[12] Chelluboina B and Vemuganti R. Chronic kidney disease in the pathogenesis of acute ischemic stroke. J Cereb Blood Flow Metab 2019; 39: 1893-1905.

[13] Bederson JB, Pitts LH, Tsuji M, Nishimura MC, Davis RL and Bartkowski H. Rat middle cerebral artery occlusion: evaluation of the model and development of a neurologic examination. Stroke 1986; 17: 472-476.

[14] Yamashita T, Kamiya T, Deguchi K, Inaba T, Zhang H, Shang J, Miyazaki K, Ohtsuka A, Ka-

tayama Y and Abe K. Dissociation and protection of the neurovascular unit after thrombolysis and reperfusion in ischemic rat brain. J Cereb Blood Flow Metab 2009; 29: 715-725.

[15] Ohta Y, Kamiya T, Nagai M, Nagata T, Morimoto N, Miyazaki K, Murakami T, Kurata T, Takehisa Y, Ikeda Y, Asoh S, Ohta S and Abe K. Therapeutic benefits of intrathecal protein therapy in a mouse model of amyotrophic lateral sclerosis. J Neurosci Res 2008; 86: 3028-3037.

[16] Sun H, Li X, Chen X, Xiong Y, Cao Y and Wang Z. Drp1 activates ROS/HIF-1α/EZH2 and triggers mitochondrial fragmentation to deteriorate hypercalcemia-associated neuronal injury in mouse model of chronic kidney disease. J Neuroinflammation 2022; 19: 213.

[17] Nih LR, Gojgini S, Carmichael ST and Segura T. Dual-function injectable angiogenic biomaterial for the repair of brain tissue following stroke. Nat Mater 2018; 17: 642-651.

[18] Block GA, Klassen PS, Lazarus JM, Ofsthun N, Lowrie EG and Chertow GM. Mineral metabolism, mortality, and morbidity in maintenance hemodialysis. J Am Soc Nephrol 2004; 15: 2208-2218.

[19] Pulskens WP, Verkaik M, Sheedfar F, van Loon EP, van de Sluis B, Vervloet MG, Hoenderop JG and Bindels RJ. Deregulated renal calcium and phosphate transport during experimental kidney failure. PLoS One 2015; 10: e0142510.

[20] Dunn DM and Munger J. Interplay between calcium and ampk signaling in human cytomegalovirus infection. Front Cell Infect Microbiol 2020; 10: 384.

[21] Woods A, Dickerson K, Heath R, Hong SP, Momcilovic M, Johnstone SR, Carlson M and Carling D. Ca2+/calmodulin-dependent protein kinase kinase-beta acts upstream of AMP-activated protein kinase in mammalian cells. Cell Metab 2005; 2: 21-33.

[22] Cantó C, Gerhart-Hines Z, Feige JN, Lagouge M, Noriega L, Milne JC, Elliott PJ, Puigserver P and Auwerx J. AMPK regulates energy expenditure by modulating NAD+ metabolism and SIRT1 activity. Nature 2009; 458: 1056-1060.

[23] Ryu DR, Yu MR, Kong KH, Kim H, Kwon SH, Jeon JS, Han DC and Noh H. Sirt1-hypoxia-inducible factor-1α interaction is a key mediator of tubulointerstitial damage in the aged kidney. Aging Cell 2019; 18: e12904.

[24] Li L, Pan H, Wang H, Li X, Bu X, Wang Q, Gao Y, Wen G, Zhou Y, Cong Z, Yang Y, Tang C and Liu Z. Interplay between VEGF and Nrf2 regulates angiogenesis due to intracranial venous hypertension. Sci Rep 2016; 6: 37338.

[25] Shibuya M. Vascular endothelial growth factor (VEGF) and its receptor (VEGFR) signaling in angiogenesis: a crucial target for anti- and pro-angiogenic therapies. Genes Cancer 2011; 2: 1097-1105.